Acc. Chem. Res. **2002,** *35,* 1070−1078

Single Nanotube Raman Spectroscopy

M. S. DRESSELHAUS,*,† G. DRESSELHAUS,‡ A. JORIO,⊗,§ A. G. SOUZA FILHO,⊗,⊥ M. A. PIMENTA,|| AND R. SAITO#

Department of Electrical Engineering and Computer Science, Department of Physics, and Francis Bitter Magnet Laboratory, Massachusetts Institute of Technology, Cambridge, Massachusetts 02139, Departamento de Física, Universidade Federal de Minas Gerais, Belo Horizonte, MG, 30123-970 Brazil, Departamento de Física, Universidade Federal do Ceará, Fortaleza, CE, 60455-760, Brazil, and Department of Electronic Engineering, University of Electro-Communications, Tokyo, 182-8585 Japan

Received January 31, 2002

ABSTRACT

A review is presented on the observation of the resonant Raman spectra from one isolated single wall carbon nanotube, focusing on the important structural information that is provided by single nanotube spectroscopy including the (*n*, *m*) determination of the individual tubes. The special sensitivity of the radial breathing mode to the (*n*, *m*) determination is emphasized, and the corroboration of this (*n*, *m*) assignment by diameter- and chirality-dependent phenomena in other Raman modes, such as the G-band, D-band, and G′-band features is also discussed. The significance of single nanotube spectroscopy for future nanotube research in general is briefly reviewed.

1. Introduction

Because of the coupling between electrons and phonons under resonant conditions, phonons or lattice vibrations provide a sensitive probe of the remarkable electronic structure of single wall carbon nanotubes (SWNTs), which are one atom in thickness, a few tens of atoms in circumference, and many micrometers in length, and can be either semiconducting or metallic, depending on their diameter and chirality.[1,2] Resonance Raman spectroscopy has played an important role in the characterization of carbon nanotubes, both in terms of the diameter distribution in SWNT bundles (an ensemble of different tubes with different diameters and chiralities) and whether a nanotube is metallic or semiconducting.[3] The possibility of obtaining a Raman spectrum from one nanotube opens new possibilities for a detailed study of the Raman spectra from SWNTs and for the use of Raman spectroscopy as a structural characterization tool for SWNTs, as is discussed in this review.

The observation of Raman spectra from just one nanotube[4] is possible because of the very large density of electronic states (number of states, ΔN, per energy range, ΔE) that occurs in this one-dimensional nanostructure at certain well-specified energies dependent on the unique geometric structure of each SWNT. When the incident or scattered photons in the Raman process are in resonance with an electronic transition between the valence and conduction bands at these special energy states, E_{ii}, the Raman signal becomes very large as a result of the strong coupling which occurs between the electrons and phonons of the nanotube under these resonance conditions.

These resonance conditions allow us to obtain a large Raman signal enhancement, and, thus, to observe, on the single nanotube level, each feature of the carbon nanotube Raman spectrum that is normally observed in SWNT bundles.[3] The possibility of single nanotube spectroscopy

* To whom correspondence should be addressed.
† Department of Electrical Engineering and Computer Science and Department of Physics, Massachusetts Institute of Technology. E-mail: millie@mgm.mit.edu.
‡ Francis Bitter Magnet Laboratory, Massachusetts Institute of Technology. E-mail: gene@mgm.mit.edu.
⊗ Department of Physics, Massachusetts Institute of Technology.
§ Present address: Departamento de Física, Universidade Federal de Minas Gerais. E-mail: adojorio@mgm.mit.edu; adojorio@cedro.fisica.ufmg.br.
⊥ Present address: Departamento de Física, Universidade Federal do Ceará. E-mail: antonio@mgm.mit.edu; agsf@fisica.ufc.br.
|| Departamento de Física, Universidade Federal de Minas Gerais. E-mail: marcos@mgm.mit.edu; mpimenta@fisica.ufmg.br.
Department of Electronic Engineering, University of Electro-Communications. E-mail: saito@mgm.mit.edu; rsaito@tube.ee.uec.as.jp.

M. S. Dresselhaus was born on November 11, 1930, in Brooklyn, NY, and received her Ph.D. degree in physics from the University of Chicago in 1958. After a two year postdoc at Cornell University, she came to MIT Lincoln Laboratory as a staff member and has been on the MIT faculty since 1967. She is an Institute Professor of Electrical Engineering and Physics at MIT with broad interest in carbon science since 1961, and has been involved in carbon nanotube research since 1991 and carbon fiber research since 1980.

G. Dresselhaus was born on November 7, 1929, in Ancon, Panama Canal Zone, and received his Ph.D. degree in physics from the University of California in 1955. He served one year as a postdoc at the University of Chicago, and four years as an assistant professor at Cornell before joining MIT Lincoln Laboratory in 1960 as a staff member. In 1977, he transferred to the MIT Francis Bitter Magnet Laboratory where he is currently a Senior Scientist. His area of interest is the electronic structure of solids. He also been broadly involved in carbon research since 1955 and carbon nanotube research since 1991, and has coauthored with M. S. Dresselhaus several books on carbon materials.

A. Jorio was born on June 11, 1972, in Brazil and received his Ph.D. degree in physics from the Federal University of Minas Gerais, Brazil, in 1999. While completing his Ph.D., he spent one year (1998) working with Dr. Roland Currat at the Laue-Langevin Institute, France. He worked for two years (2000 and 2001) with Professor M. S. Dresselhaus at MIT as a postdoctoral fellow. He is currently an Associate Professor of Physics at the Federal University of Minas Gerais.

A. G. Souza Filho was born on June 12, 1975, in Brazil and received his Ph.D. degree in physics from the Federal University of Ceará, Brazil, in 2001. In 2001, he joined the Dresselhaus group at MIT as a Ph.D. visiting student, where he worked for 10 months on single carbon nanotube Raman spectroscopy. He is currently an associate researcher at the Federal University of Ceará working on aspects of Raman scattering in solids.

Marcos Pimenta was born on April 11, 1958, in Belo Horizonte, Brazil, and received his Ph.D. degree in physics from the Université d'Orleans, France, in 1987. In 1997−1998 he spent a sabbatical year with Professor Dresselhaus at MIT. He is a full Professor of Physics at the Federal University of Minas Gerais and a Co-Director of the Institute of Nanoscience at UFMG−Brazil. He has made important contributions to Raman spectroscopy of carbon nanotubes.

R. Saito was born on March 13, 1958, in Tokyo. He graduated (B.S.) from Tokyo University and earned his Ph.D. there in 1985. After being a research associate at Tokyo University, Saito has been an associate professor at the University of Electro-Communication in Tokyo since 1990. He has worked intensively on the theory of carbon nanotubes since 1991, and has written a book on the subject in collaboration with G. and M. S. Dresselhaus, *Physical Properties of Carbon Nanotubes*, published by Imperial College Press, in 1998. He was the recipient of the Japan IBM prize in 1999.

10.1021/ar0101537 CCC: $22.00
Published on Web 07/11/2002

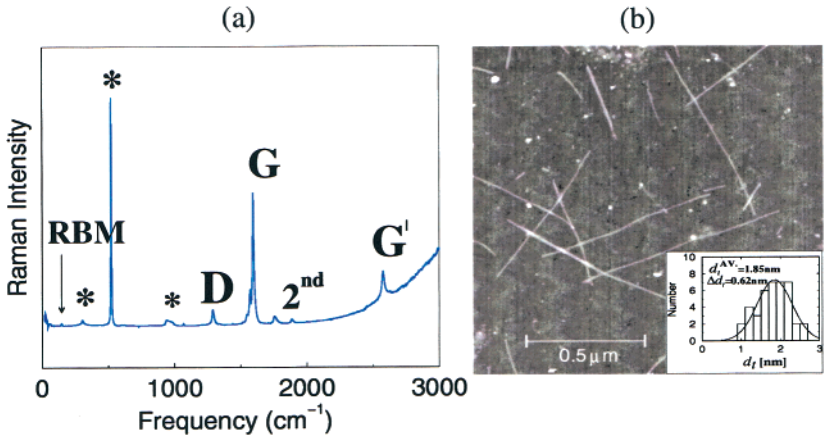

FIGURE 1. (a) Raman spectrum from one nanotube taken over a broad frequency range using E_{laser} = 785 nm = 1.58 eV excitation and showing the radial breathing mode (RBM), the D-band, the G-band, and the G′-band. Second-order (2nd) modes are also observed, but are not discussed in this review. The features marked with an asterisk (*) at 303, 521, and 963 cm^{-1} are from the Si/SiO_2 substrate[6] and are used for calibration of the nanotube Raman spectrum. (b) AFM image of the sample showing isolated single wall nanotubes grown from the vapor phase.[7] The small particles are iron catalyst particles. The inset shows the nanotube diameter distribution of this sample ($d_t = 1.85 \pm 0.62$ nm) based on AFM observations of 40 SWNTs.[4]

allows us to study the dependence of each Raman feature on nanotube diameter and chirality (chiral angle), as well as to obtain information about the intensity, line width, and polarization properties of each feature, its dependence on laser excitation energy, and finally, the connection between spectra at the single nanotube level and Raman spectra normally observed from SWNT bundles.

Since the observation of the Raman spectrum from one nanotube depends on a resonance between the incident or scattered photon with an electronic transition, E_{ii},[5] the resonance process is highly selective of particular SWNTs, since each SWNT, characterized by two integer indices (n, m), has a unique set of such electronic transitions energies, E_{ii}. Since the geometrical structure of each nanotube (namely its diameter, d_t, and the orientation of the hexagons of carbon atoms with respect to the nanotube axis, denoted by the chiral angle θ) is intimately connected to these same indices (n, m),[1,2] we can consider each set of (n, m) indices to define a unique giant molecule, and every distinct molecule to have its own unique electronic and Raman spectrum. Resonance Raman spectroscopy at the single nanotube level thus becomes a structural characterization tool, as in molecular spectroscopy, that can distinguish each molecular species through its unique Raman spectrum.

The isolated SWNTs used in these single nanotube Raman experiments were prepared by a chemical vapor deposition method on a Si substrate containing nanometer-sized iron catalyst particles. Since the Si substrate forms a thin SiO_2 surface coating, the interaction between the SWNTs and the substrate is expected to be weak. Since the nanotubes nucleate and grow from well-isolated catalyst particles, nanotube bundles are not formed. Figure 1b shows an atomic force microscopy (AFM) image of a sample with a high SWNT concentration (6 ± 3 SWNTs/μm^2), shown here for easy visualization. The inset to Figure 1b shows the wide diameter distribution of the SWNT samples ($1 < d_t < 3$ nm) typically used in these studies. For quantitative studies at the single nanotube level, dilute samples with SWNT densities of <1 SWNT/μm^2 are used to ensure that the actual Raman spectra are for an individual isolated carbon nanotube and that the various features observed in the spectrum come from one and the same resonant nanotube.

Resonance Raman spectra in the 100−3000 cm^{-1} spectral range from these individual isolated SWNTs are taken with a readily available Raman microprobe instrument, such as a Renishaw Raman Microprobe (1-μm laser spot), using laser excitation with ~10 mW power, such as E_{laser} = 514.5 nm = 2.41 eV, readily obtainable from an argon ion laser. The Raman spectrum shown in Figure 1a was taken with a Kaiser micro-Raman spectrograph operating at E_{laser} = 785 nm = 1.58 eV. Relatively high laser powers can be used to probe isolated SWNTs without substantial heating effects because of their unusually high thermal conductivity,[8] their excellent high-temperature stability and robustness (up to ~30 mW on 1 μm^2), and their good thermal contact to the substrate.

The basic theory allowing the observation of Raman spectra from one nanotube and the use of these spectra for structural (n, m) determination at the single nanotube level is discussed in section 2, whereas section 3 reviews how the radial breathing mode feature is used to determine (n, m) and to give the profile for the van Hove singularity in the joint density of states. The corroboration of the (n, m) assignment by the diameter- and chirality-dependent features in the G-band, D-band, and G′-band are reviewed in section 4, whereas section 5 concludes the Account and sets the importance of single nanotube spectroscopy in a larger context.

2. Basic Theory

A single wall carbon nanotube can be considered to be a single atomic layer of 2D graphite (called a graphene sheet) rolled up into a seamless cylinder. The structure of each nanotube is uniquely described by two integers (n, m), which refer to the number of $\vec{a}_1$ and $\vec{a}_2$ unit vectors

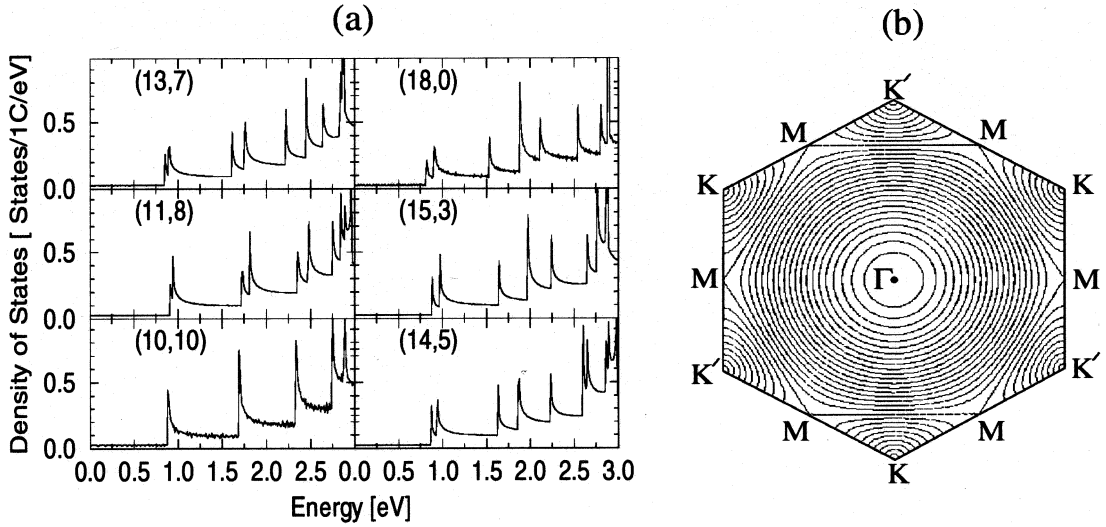

FIGURE 2. (a) 1D electronic density of states (DOS) vs energy (measured from the Fermi level) for six metallic nanotubes of approximately the same diameter, where the density of states denotes the number of quantum states per energy range. The plots for the six tubes with different (*n*, *m*) values show the effect of chirality and trigonal warping (see text) on the van Hove singularities in the density of states. The (10, 10) (armchair) tube has no trigonal warping effect and the (18, 0) (zigzag) tube has the maximum effect. Only the densities of states for the conduction π^* band are shown; the mirror image of these plots gives the electronic DOS for the valence π band[9,10] within the tight binding approximation,[2] assuming the energy overlap integral is $\gamma_0 = 2.9$ eV and the wave function overlap integral vanishes $s = 0$. (b) Plot of the 2D equienergy contours of 2D graphite, showing trigonal warping effects in the contours, as we move away from the *K* point in the $K-\Gamma$ or $K-M$ directions. The equienergy contours are circles near the *K* point and near the center of the Brillouin zone, where no trigonal warping is present. But near the M points on the zone boundary, the contours that connect the nearest *M* points are straight lines and show very large trigonal warping effects.[9]

of the 2D graphene lattice that are contained in the chiral vector, $\vec{C}_h = n\vec{a}_1 + m\vec{a}_2$, which spans the circumference of each nanotube.[2] From the (*n*, *m*) indices, one can calculate the nanotube diameter d_t, the chirality or chiral angle θ, the electronic energy bands, and the density of electronic states,[2] as well as the energies of the interband transitions $E_{ii}(n, m)$ between the so-called van Hove singularities in the valence and conduction band density of states, as shown in Figure 2a, where the intensities in the density of states is very high. Because of the trigonal warping effect of the electronic energy bands of 2D graphite shown in Figure 2b, there is a weak dependence of the electronic energy levels of SWNTs on chiral angle θ, as well as a much stronger dependence on nanotube diameter d_t, which determines the number of carbon atoms in the circular cross-section of the nanotube shell, one atom in thickness.[2]

The weak dependence of the electronic energy bands of SWNTs on chiral angle θ relates to the 3-fold symmetry of the electronic dispersion relations about the *K*-point of the 2D graphene Brillouin zone (see Figure 2b), where the graphene valence and conduction bands are degenerate, forming a zero-band gap semiconductor.[2] Away from the *K*-point, the graphene electronic energy bands exhibit a trigonal warping effect,[9] as shown in Figure 2b, and this trigonal warping effect is responsible for the unique spectrum of singularities in the density of states of the conduction and valence bands for each (*n*, *m*) SWNT when the energy bands of the graphene lattice are zone-folded to form the energy bands of the SWNTs.[2,9] The chirality dependence of the van Hove singularities[9,10] in the 1D electronic density of states (DOS) of the conduction band, where the energy measured relative to the Fermi energy, is shown in Figure 2a for several metallic (*n*, *m*) nanotubes, all having about the same diameter d_t (from 1.31 to 1.43 nm), but having different chiral angles: $\theta =$ 0, 8.9, 14.7, 20.2, 24.8, and 30.0° for nanotubes (18, 0), (15, 3), (14, 5), (13, 7), (11, 8), and (10, 10), respectively. The plot shows that as the chiral angle is varied from the armchair nanotube (10, 10) ($\theta = 30°$) to the zigzag nanotube (18, 0) ($\theta = 0°$), a splitting due to the trigonal warping effect (see Figure 2b) develops in all of the singularities in the DOS,[9,10] and this splitting due to trigonal warping increases with decreasing chiral angle. Since the peak energies in the density of states (see Figure 2a) are unique for each (*n*, *m*) value, the interband transition energies, E_{ii}, are also unique. For carbon nanotubes, interband transitions are strongly favored when the photon energy excites an electron from the *i*th peak in the valence band density of electronic states to the *i*th peak in the conduction band density of states, corresponding to vertical transitions in the extend zone (2D graphene). The peak energies, E_{ii}, give rise to a unique set of singularities in the joint density of states (JDOS) for each (*n*, *m*) value, where E_{ii} occurs at twice the energy of the singularities shown in Figure 2a. A plot of the singularities in the JDOS denoted by E_{ii} is presented in Figure 3a as a function of nanotube diameter d_t.[11] Reliable values of E_{ii} are obtained by the tight binding approximation for $0.7 < d_t < 2.3$ nm.

As can be seen in Figure 3a, the trigonal warping effect causes a spread of the interband energies, E_{ii}, between the singularities in the JDOS for nanotubes with the same diameter d_t. Here the integer *i* labels the singularities in

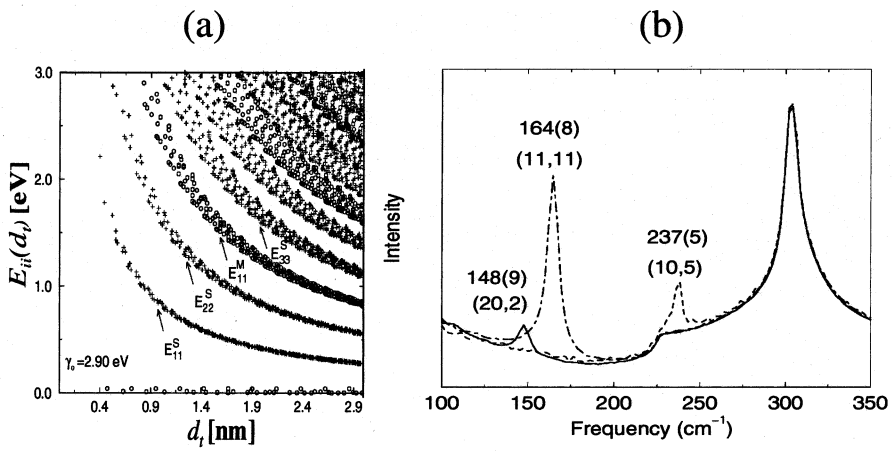

FIGURE 3. (a) Calculated[11] energy separations E_{ii} between van Hove singularities i in the 1D electronic density of states of the conduction and valence bands for all (n, m) values vs nanotube diameter $0.4 < d_t < 3.0$ nm, using a value for the carbon−carbon energy overlap integral of $\gamma_0 = 2.9$ eV and a nearest neighbor carbon−carbon distance $a_{C-C} = 1.42$ Å.[9,12] Semiconducting (S) and metallic (M) nanotubes are indicated by crosses and open circles, respectively. The index i in the interband transitions E_{ii} denotes the transition between the van Hove singularities, with $i = 1$ being closest to the Fermi level taken at $E = 0$. (b) The three Raman spectra (solid, dashed, and dash−dotted curves) come from three different spots on the Si substrate, showing the presence of only one resonant nanotube and one RBM frequency for each of the three laser spots. The RBM frequencies (widths) in cm^{-1} and the (n, m) assignments for each resonant SWNT are displayed. The shoulder at 225 cm^{-1} and the 303 cm^{-1} feature come from the Si substrate and are used for calibration of the SWNT spectra.[4]

the JDOS and their energies relative to the Fermi level E_F. From the above discussion, we conclude that each nanotube (n, m) has a unique set of interband energies, E_{ii}, denoting the energy differences between the ith van Hove singularities in the conduction and valence bands, and conversely, if one interband energy, E_{ii}, and a nanotube diameter, d_t, are specified, then its corresponding unique (n, m) can in general be identified, except for a possible but rare energy degeneracy for one transition energy E_{ii} value occurring for more than one tube.

It is well-established[2] that the (n, m) indices are crucial to the nanotube electronic structure. Specifically, the SWNTs for which $|n - m| = 3q$ are metallic, and those for which $|n - m| = 3q \pm 1$ are semiconducting, where q is an integer.[1,2] Thus, we see that two-thirds of the bands in Figure 3a correspond to semiconducting nanotubes (S), and one-third are metallic (M). Nevertheless, it has proven difficult to measure (n, m) experimentally and then to carry out property measurements on the same SWNT. We explain in the next section how the resonant Raman spectra from one isolated nanotube (such as shown in Figure 1a and in Figure 3b) can conveniently provide this information. As stated above, every possible nanotube denoted by (n, m) has a distinct electronic and vibrational spectrum, so that there is a one-to-one relation between (n, m) and the singularities in the 1D joint electronic density of states.[2] As stated in the Introduction, a large enhancement in the Raman signal occurs in the resonance Raman effect, when the incident or scattered photon is in resonance with a singularity in the 1D JDOS of the SWNT, allowing the observation of a well-resolved Raman signal from an individual SWNT, as shown in Figure 3b. This figure shows three different Raman spectra in the low-frequency radial breathing mode region taken for three different isolated SWNTs, each within a different light spot ~1 μm in diameter, on a sample of isolated SWNTs, such as in Figure 1b. It is noteworthy that the Raman intensity from a strongly resonant tube, such as the (11, 11) SWNT in Figure 3b, is comparable to that from the Si substrate, even though the SWNT signal comes from only a small fraction of the number of C atoms relative to the number of substrate Si atoms (C/Si ~10^{-6}) within the optical beam. This high sensitivity for SWNTs in resonance with the incident photon is the basis for research on the Raman spectra from a single nanotube. In the next section, we explain how Raman spectra at the single nanotube level can be used to carry out the (n, m) identification for that resonant SWNT.

3. Structural (n, m) Characterization

The determination of the geometrical structure of a nanotube in terms of the indices (n, m) depends on finding the nanotube diameter and transition energy, E_{ii}, in accordance with the so-called Kataura plot, shown in Figure 3a. All features of the Raman spectra (Figure 1a) are sensitive to (n, m), including the radial breathing mode (in which all the carbon atoms are moving in-phase in the radial direction), the G-band (where neighboring atoms are moving in opposite directions along the surface of the tube as in 2D graphite), the dispersive disorder-induced D-band, and its second-order related harmonic G′-band. Although all four of these Raman features in the SWNT spectra are sensitive to (n, m), it is the radial breathing mode (RBM) that is most sensitive, and it is therefore the RBM that is used to make the initial (n, m) identification, which can then be corroborated by examination of other spectral features, as discussed below.

We first discuss how the RBM provides a convenient method for the determination of both d_t and E_{ii} from the Kataura plot of Figure 3a, thereby yielding the (n, m) identification. Regarding the determination of d_t, the RBM

frequency, ω_{RBM}, has been shown to depend linearly on the reciprocal of the nanotube diameter d_t according to the relation[2,3]

$$\omega_{RBM} = \alpha/d_t \quad (1)$$

and to be independent of chiral angle θ, as has been shown experimentally[5] and by both force constant[13] and ab initio calculations.[14,15] Theoretical determinations have been made of the proportionality constant α based on density functional theory ($\alpha = 232 \pm 10$ cm^{-1} nm),[14,15] whereas for SWNTs on the Si/SiO_2 substrate used in the experimental single nanotube spectroscopy studies, α is experimentally found to be 248 ± 2 cm^{-1} nm by the measurement of the RBM on a large number (42) of isolated semiconducting and metallic SWNTs in the process of making a self-consistent evaluation of their (n, m) indices.[4]

Regarding the determination of E_{ii}, if a tunable laser could be tuned to bring E_{laser} in perfect resonance with E_{ii} (which would then be detected as the E_{laser} value where the maximum intensity in the Raman spectrum occurs), then a simple measurement of ω_{RBM} (yielding d_t) to identify the index i in E_{ii} (see Figure 2a) would be sufficient to determine (n, m). In practice, such a tunable laser system has thus far been applied only to single nanotube Raman spectroscopy studies over a small energy range ($\sim$0.15 eV),[16] and an (n, m) determination could then be made accurately.

However, this experiment with a tunable laser went much further and provided an experimental determination of the spectral profile of the 1D joint density of states (JDOS) for a single wall carbon nanotube near a van Hove singularity, thereby giving direct evidence for the sharp singularities in the JDOS, and showing how it is possible to get sufficient intensity to observe a Raman spectrum from just one nanotube.[16] The JDOS spectral profile and the (n, m) value of the SWNT were both determined by measuring the resonant Stokes (S) and anti-Stokes (AS) Raman spectrum for this nanotube for many different frequencies, thus obtaining a reliable determination of E_{ii} to $\pm$3 meV as well as the parameters of the spectral profile (Figure 4). The experiments are carried out on a sample containing lithographic markers, so that as E_{laser} is tuned, the microscope focus can always be brought to the same nanotube. The RBM integrated intensity $I(E_{laser})$ is a function of E_{laser} and can be evaluated from the joint density of states $g(E)$ according to

$$I(E_{laser}) = \int \left| \frac{M}{(E_{laser} - E - i\Gamma_r)(E_{laser} \pm E_{ph} - E - i\Gamma_r)} \right|^2 g(E)\, dE \quad (2)$$

in which the first and second factors in the denominator, respectively, describe the resonance effect with the incident and scattered light, where the + (−) applies to the AS (S) process for a phonon of energy E_{ph}, and Γ_r gives the inverse homogeneous lifetime for the resonant scattering process and includes contributions from many processes, such as internal relaxation, possible vibronic

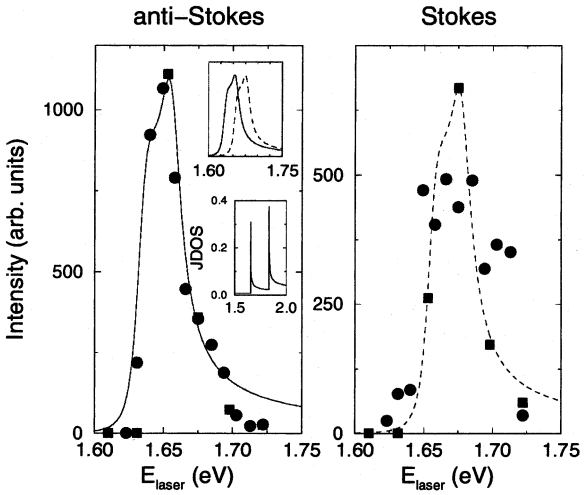

FIGURE 4. Raman intensity vs laser excitation energy E_{laser} for the $\omega_{RBM} = 173.6$ cm^{-1} peak in the Stokes (S) and anti-Stokes (AS) Raman processes of an isolated (18, 0) SWNT, where the AS intensity is normalized by $\exp(\hbar\omega_{RBM}/k_BT)$ to facilitate comparisons with the S profile. The line curves indicate the resonant Raman windows predicted from eqs 2 and 3, with $E_{ii} = 1.655$ eV, $\Gamma_r = 8$ meV, and $\Gamma_J = 0.5$ meV. The upper inset compares the theoretically predicted S and AS resonant windows. The lower inset plots the JDOS profile for the two lowest energy van Hove singularities for one isolated (18, 0) SWNT with $\Gamma_J = 0.5$ meV.[16]

phonon structure in E_{ii}, temperature-broadening effects, and coupling with the radiation field. The matrix element in eq 2 for the scattering process $M = M_i M_{ep} M_s$ is for simplicity considered to be independent of E. Here M_i, M_s, and M_{ep} are, respectively, matrix elements for the electron-radiation absorption, the electron-radiation emission, and the electron−phonon interaction, whereas the JDOS profile $g(E)$ can be approximated within the one-electron theory by the asymmetric profile

$$g(E) = \mathrm{Re}\left[\sum_i \frac{a_{C-C}E}{d_t\gamma_0\sqrt{[(E - E_{ii} - i\Gamma_J)(E + E_{ii} + i\Gamma_J)]}} \right] \quad (3)$$

where $a_{C-C} = 1.42$ Å is the nearest-neighbor distance between carbon atoms, γ_0 is the tight binding energy overlap integral, and Γ_J is introduced as a measure of the effect on the width of the JDOS singularity for the E_{ii} electronic transition of the nanotube finite length and of the finite size of the laser beam on the nanotube, reflecting a finite number of effective wave vectors along the tube length. To some extent, Γ_J depends on the characteristics of the individual SWNT, but should have approximately the same value from one tube to another. Values of $\gamma_0 = 2.90 \pm 0.02$ eV and $\Gamma_J = 0.7 \pm 0.3$ meV provide a good fit to a large body of experimental data. The sum over i takes into account the different van Hove singularities of one SWNT (see Figure 3a).

Experimentally, a fit of the data points in Figure 4 determines the values of the fitting parameters in eqs 2 and 3, showing that Γ_r is most sensitive to determining the fwhm (full width at half-maximum intensity) line width of the spectral features, but that the very small value of Γ_J ($\sim$0.7 meV) gives rise to the very strong intensity

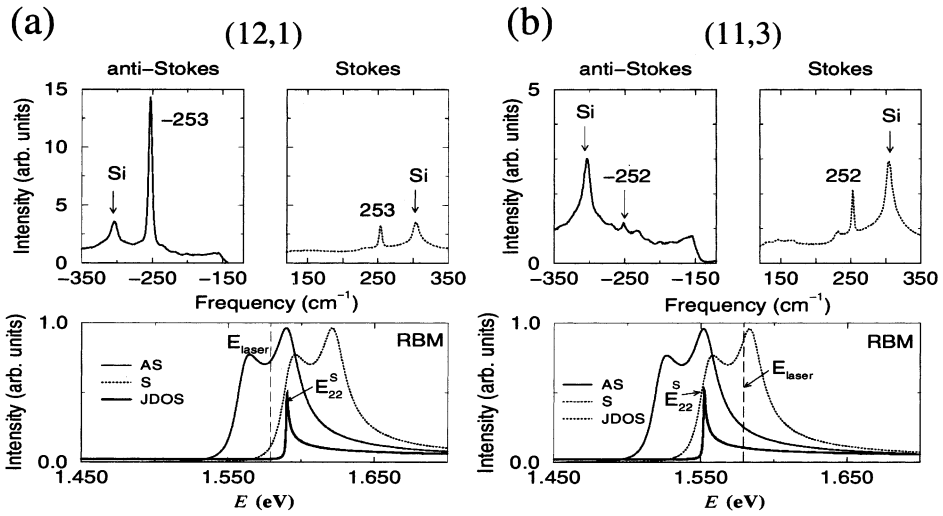

FIGURE 5. (a) Resonance anti-Stokes (AS) and Stokes (S) spectra for a (12, 1) semiconducting SWNT on a Si/SiO_2 substrate using 1.579 eV (785 nm) laser excitation (upper panels) and the predicted joint density of states (heavy line) and resonant windows for the RBM mode in the anti-Stokes (solid line) and Stokes (dotted line) processes for the (12, 1) SWNT (lower panel). Part (b) is the same as in (a), except that the data are for the (11, 3) SWNT. The energy E_{22}^S in (a) and (b) in the lower panels is varied to obtain the experimentally measured I_{AS}/I_S ratio given in the upper panels of (a) and (b) where the AS spectra are normalized by the Boltzmann factor for easy comparisons of the relative AS and S intensities.

enhancement (∼1000) associated with the sharp 1D van Hove singularities in the joint density of states $g(E)$. Once the parameters in eqs 2 and 3 are found, the spectral profile of the JDOS can be plotted, as in the inset to Figure 4, where $g(E)$ is seen to be highly asymmetric and to have very sharp singularities, with a width of <1 meV. Measurements of the Stokes and anti-Stokes spectra over the whole resonance window of the nanotube yield the E_{ii} value more accurately (to 3 meV) than when using a single laser line (∼10 meV accuracy).

Many physical properties, such as transport, optical, and mechanical properties, are very sensitive to the spectral profile of the electronic density of states, but the profile is difficult to measure directly, because probes, such as scanning tunneling microscopy (STM) tips,[17] interact too strongly with the nanotube, thereby broadening the van Hove singularities (from <1 to >10 meV), and consequently also broadening the density of states that is probed by scanning probe methods.[17]

Even though a tunable laser is not generally available, nevertheless, an (n, m) determination for an isolated SWNT can in most cases be made if a nanotube is within the resonant window of a single available laser excitation line, which in practice is satisfied for E_{laser} within ∼±0.1 eV of an interband transition for that nanotube. From the measured ω_{RBM} and use of eq 1, the nanotube diameter, d_t, is found, and the i index in E_{ii} can be found from Figure 2a. The more challenging measurement is the determination of the value of E_{ii}.

One method to determine the value of E_{ii} directly requires measurement of both the Stokes and anti-Stokes radial breathing mode spectra.[18,19] This procedure is very important when the ω_{RBM} values for two or more SWNTs (or consequently the d_t values for two or more SWNTs) are very close to each other, as happens, for example, for the semiconducting tubes (12, 1) and (11, 3) shown in Figure 5a and b, respectively. The use of eq 1 for these tubes yields d_t values very close to one another so that it is not possible to distinguish between them from the measured d_t values. However, the ratio of the anti-Stokes-to-Stokes intensities, I_{AS}/I_S, for the radial breathing mode is very different for the two nanotubes, as seen in Figure 5, and this large difference in I_{AS}/I_S is then used to sensitively (to 10 meV accuracy) determine the energy E_{ii} of the resonant van Hove singularity in the joint density of states (lower panels in Figure 5).[18] This determination is done by calculating the experimental E_{ii}^{expt} that would produce the measured I_{AS}/I_S ratio. The (n, m) is determined as the best fit of the measured d_t and E_{ii}^{expt} to the predicted d_t and E_{ii} values for a given (n, m) (lower panels in Figure 5), thereby providing an experimental determination of the (n, m) indices unambiguously. This is illustrated in Figure 5 above for the tubes (12, 1) and (11, 3), which have very similar d_t values but very different experimental E_{22}^S values of 1.587 and 1.554 eV, respectively, to be compared to their corresponding theoretical values of 1.585 and 1.564 eV.

In practice, the (n, m) index characterization for isolated nanotubes can be simply carried out by using a single laser excitation energy E_{laser} when the nanotube is in resonance with E_{laser}, making use of the intensity of the radial breathing mode, the calculated E_{ii} values of various candidate (n, m) nanotubes, and a comparison between the relative RBM intensities of the test SWNT and the intensities of other SWNTs whose (n, m) indices have previously been determined (and consequently, also their experimentally determined d_t and E_{ii} values have been matched to calculated values.) If the (n, m) values of every nanotube in the sample must be found, then a tunable laser is needed to provide a resonant excitation energy for each nanotube so that a complete (n, m) Raman characterization can be carried out for each SWNT.

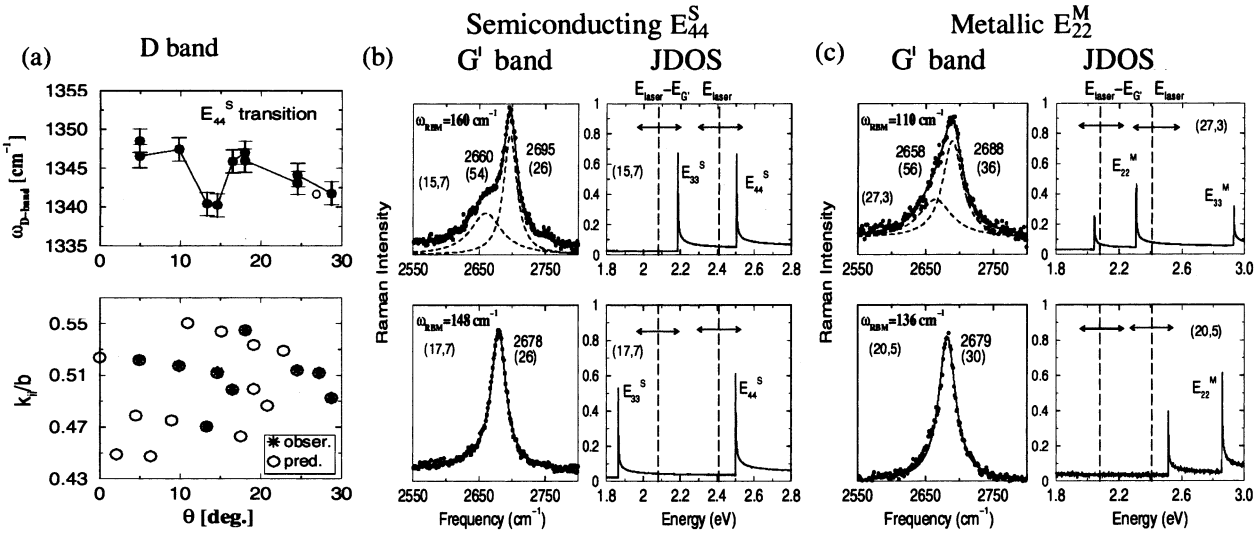

FIGURE 6. (a) Measured *D*-band frequencies as a function of chiral angle θ of semiconducting SWNTs for which E_{laser} is in resonance with the E_{44}^S interband transitions (upper panel) and the distance $|k_{ii}|$ to the *K* point for electrons in the 2D Brillouin zone of graphite (see Figure 2b), associated with the E_{ii} van Hove singularities, plotted as open circles vs θ for the possible resonant tubes (lower panel) and as stars over the open circles for the experimentally observed tubes in the upper panel. (b) *G*′-band profile (left panel) and joint density of electronic states (right panel) for the (15, 7) and (17, 7) SWNTs. The vertical dashed lines at 2.41 and 2.08 eV are for the incident and scattered photons, respectively. The horizontal double arrows denote the resonant windows for the incident and scattered photons. All frequencies (line widths) are in units of cm^{-1}. (c) Same as in (b), except that the data are for the (27, 3) and (20, 5) metallic SWNTs.

4. Corroboration of the (*n*, *m*) Assignments

Every one of the other features in the Raman spectra from individual SWNTs, namely the G-band, the D-band, and the G′-band, are sensitive to (*n*, *m*) and, therefore, can be used to check the (*n*, *m*) assignment discussed in Section 3, although none of these features is as sensitive to (*n*, *m*) as the radial breathing mode. Thus, the other features are used for corroborating (*n*, *m*) and to check for possible blunders that could have been made in the initial (*n*, *m*) identification implied by the RBM feature.

As shown by recent measurement, the difference in the G-band line shape between metallic and semiconducting nanotubes can be observed at the single nanotube level for nanotube diameters ≤2.2 nm,[20] thus providing a direct validation on the difference ($n - m$). The G-band is dominated by two higher-intensity peaks (see Figure 1a) denoted by G^+ and G^-. The splitting between the frequency of the upper and lower G-band peaks provides a determination of d_t through the relation $\omega_G^- = \omega_G^+ - \mathcal{C}/d_t^2$ where $\mathcal{C} = 45.8$ cm^{-1} nm^2 for semiconducting tubes and 79.5 cm^{-1} nm^2 for metallic nanotubes.[20] The strong polarization effects observed for the RBM and G-band features point to the importance of monitoring the polarization alignment with respect to the nanotube axis when doing (*n*, *m*) characterization.[21] Finally, for special (*n*, *m*) values, when using a specific E_{laser} excitation, it is possible for the incident photon to be in resonance with one E_{ii} value (for example, E_{44}^S) and for the scattered photon to be in resonance with another E_{ii} value (for example, E_{33}^S), and unusual G-band profiles are then observed. Such a situation is extremely sensitive (at the meV level) to the (*n*, *m*) identification and provides sensitive corroboration for a given (*n*, *m*) assignment.[20]

Other Raman modes that can be used to further corroborate the (*n*, *m*) identification are the dispersive bands (see Figure 6) (the disorder-induced D-band and the second-order *G*′-band). In Raman experiments in general, the phonon frequency does not depend on the laser excitation energy (as, for example, for the RBM band and the G-band). The D-band and G′-band are special, because they change in frequency when the laser excitation energy changes; i.e., these bands are dispersive. The origin of this dispersive behavior[3,5,22] in both graphite and single wall carbon nanotubes[23,24] has been explained by a double resonance Raman process involving a second-order scattering process and a Raman intensity enhancement due to the resonance with both an intermediate state and resonance with either the initial or final states, thus yielding a double resonance process, giving rise to a special electron−phonon coupling. In the case of nanotubes, the quantized wave vectors k_{ii} play a fundamental role in determining the resonant process, as is clearly seen when we plot the chiral angle-dependence of ω_D, as shown in the upper left panel of Figure 6a. The corresponding k_{ii} in the lower panel of Figure 6a denote the wave vectors for the confined electronic states in the van Hove singularities. In the lower panel of Figure 6a, the circles denote the predicted (*n*, *m*) indices that can be resonant, and the crosses denote the SWNTs that were actually observed in the Raman experiments carried out to date. The good agreement between upper and lower panels in Figure 6a shows that the θ dependence of ω_D in SWNTs can be explained in terms of the relation between $|k_{ii}|$ for electrons and q for phonons to which electrons are strongly coupled by the double-resonance process. The similar patterns, as a function of chirality θ for the electron wave vectors k_{ii} and the observed ω_D phonon frequencies,

tell us that the (n, m) assignment is reliable, for otherwise $\omega_D(\theta)$ and k_{ii} would not be correlated with each other as they indeed are.

The large dispersion of the G'-band mode is important for providing information about the electronic structure of the nanotubes. Since the double-resonance process is constrained by the van Hove singularities in the 1D SWNT JDOS, the G'-band profile is strongly dependent on the electronic structure and then can be used to corroborate the (n, m) assignment for a resonant SWNT. The G'-band for most of the semiconducting tubes shows a single Lorentzian peak, as in the lower left panel of Figure 6b. However, some SWNTs show a "two peak effect", as in the upper left panel of Figure 6b. These different G'-band profiles can be understood by analyzing the resonant process of E_{laser} with the singularities in the JDOS shown in the right panels of Figure 6b, keeping in mind that the quantized states k_{ii} determine the G'-band frequencies $\omega_{G'}$. By examining the JDOS we see that for the (15, 7) SWNT, E_{laser} (incident photon) is resonant with E_{44}^S and $E_{laser} - E_{G'}$ (scattered photon) is resonant with E_{33}^S in a resonance that occurs as two independent processes. Then, the double peak observed for (15, 7) arises from resonance processes involving k_{44} (upper frequency component) and k_{33} (lower frequency component).

The G'-band profile in the lower left panel of Figure 6b has a single Lorentzian peak, because only the incident photon is resonant. It is just this profile that, indeed, allows the identification of this tube as (17, 7), since the singularity E_{33}^S is too far from the energy of the scattered photon to allow the resonance to occur. From the measured $\omega_{RBM} = 148$ cm^{-1}, there are two likely (n, m) candidates for this tube, namely, the (17, 7) and (16, 8) SWNTs. The (16, 8) is eliminated from the assignment, because the E_{33}^S energy would give rise to a strong resonance with the scattered photon, and two peaks in the G'-band would then be expected. We thus conclude that the $\omega_{RBM} = 148$ cm^{-1} SWNT here corresponds to (17, 7).

The "two peak" effect in the G'-band spectrum is also observed in metallic tubes, as can be observed in the lower left panel of Figure 6c. Some single Lorentzian peak profiles are also observed. The two peaks in the G'-band for metallic tubes are associated with the splitting of the electronic states ΔE_{ii}^M due to trigonal warping effects, being zero for armchair SWNTs and a maximum for zigzag SWNTs (see Figure 2a). Since different electronic energies occur for each component of the ΔE_{ii}^M pair (see Figure 3a), different k_{ii} vectors will result, thereby giving rise to different phonon wave vectors q for the G' band phonons and, finally, to different $\omega_{G'}$ values denoted by $\Delta\omega_{G'}$, as observed in the lower left panel of Figure 6c for the (27, 3) nanotube. The (20, 5) SWNT has a G'-band with a single Lorentzian line shape for $E_{laser} = 2.41$ eV excitation, in agreement with its JDOS, for which the only resonance is for the incident photon with the lower E_{ii}^M component, as shown in the figure. This is not the case for the (27, 3) tube, where a two peak effect in the G'-band profile is observed experimentally, in agreement with the calculated JDOS for this tube. Armchair tubes (n, n) do not show trigonal warping-induced splittings in E_{ii}^M [see, for example, the (10,10) tube in Figure 2a], so that the (15, 15) tube, which is predicted to be resonant with $E_{laser} = 2.41$ eV, should show a G'-band with a single Lorentzian line shape, in good agreement with experiment.

By measuring these splittings, $\Delta\omega_{G'}$ in the $\omega_{G'}$ profiles for SWNTs with different chirality, it is possible to determine the dependence of $\Delta\omega_{G'}$ on ΔE_{ii}^M. The linear relation observed experimentally for $\Delta\omega_{G'}$ vs ΔE_{ii}^M gives an independent determination of 108 ± 5 cm^{-1}/eV for the dispersion of $\omega_{G'}$ as a function of E_{laser}, even though the measurements are all made using one laser line.[25] The agreement between this determination of the dispersion of $\omega_{G'}$ vs E_{laser} with direct measurements of $\omega_{G'}$ for SWNT bundles as a function of E_{laser} gives further corroboration for the (n, m) structural determination of these SWNTs using resonance Raman spectroscopy.

Conclusions

A brief review of single nanotube Raman spectroscopy is here presented, emphasizing in particular how such spectra can be observed and the use of these spectra for the structural (n, m) determination of individual nanotubes. The special high sensitivity of the radial breathing mode feature for the structural determination is emphasized, but the use of diameter- and chirality-sensitive aspects of the other spectral features, such as the G-band, D-band, and G′-band, allow corroboration of the (n, m) assignments made by analysis of the RBM feature. Single nanotube spectroscopy opens up a variety of research opportunities that have been largely unexplored until now, including understanding in detail the diameter- and chirality-dependence of the Raman spectra from SWNT bundles, and the use of Raman structural (n, m) characterization of isolated SWNTs that can then be investigated for their diameter- and chirality-dependent mechanical, elastic, optical, transport, thermal, and emission properties. Finally, Raman spectra of carbon nanotubes at the single nanotube level provide a model system for studying the special characteristics of Raman spectroscopy of 1D systems.

A.J. and A.G.S.F. acknowledge financial support from the Brazilian agency CNPq under PROFIX and DCR contracts, respectively. The authors thank Prof. C. M. Lieber and Dr. J. H. Hafner of Harvard University for providing the samples of isolated SWNTs used in the experiments, and Prof. Anna Swan of Boston University for fruitful discussions. Acknowledgments are gratefully made to the Photonics Center of Boston University operated in conjunction with their Department of Physics and the Department of Electrical and Computer Engineering, where part of the experimental work was performed. This work also made use of the MRSEC Shared Facilities at MIT, supported by the National Science Foundation under Grant DMR-9400334 and NSF Laser facility Grant No. 97-08265-CHE. The MIT authors acknowledge support under NSF Grants DMR 01-16042 and INT 98-15744. The collaboration between the Brazilian and MIT authors is facilitated by the jointly funded Brazil−U.S. Research program (NSF INT 00-00408 and

CNPq 910120/90-4). R.S. acknowledges a Grant-in-Aid (No. 13440091) from the Ministry of Education, Japan.

References

(1) Dresselhaus, M. S.; Dresselhaus, G.; Eklund, P. C. *Science of Fullerenes and Carbon Nanotubes*; Academic Press: New York, San Diego, 1996.

(2) Saito, R.; Dresselhaus, G.; Dresselhaus, M. S. *Physical Properties of Carbon Nanotubes*; Imperial College Press: London, 1998.

(3) Dresselhaus, M. S.; Eklund, P. C. Phonons in Carbon Nanotubes. *Adv. Phys.* **2000**, *49*, 705−814.

(4) Jorio, A.; Saito, R.; Hafner, J. H.; Lieber, C. M.; Hunter, M.; McClure, T.; Dresselhaus, G.; Dresselhaus, M. S. Structural (*n*, *m*) determination of isolated single wall carbon nanotubes by resonant Raman scattering. *Phys. Rev. Lett.* **2001**, *86*, 1118−1121.

(5) Dresselhaus, M. S.; Dresselhaus, G.; Jorio, A.; Souza Filho, A. G.; Saito, R. Raman Spectroscopy of Isolated Single Wall Carbon Nanotubes. *Carbon* **2002**, in press.

(6) Temple, P. A.; Hathaway, C. E. Multiphonon Raman Spectrum of Silicon. *Phys. Rev. B* **1973**, *7*, 3685−3697.

(7) Hafner, J. H.; Cheung, C. L.; Oosterkamp, T. H.; Lieber, C. M. High yield fabrication of single-walled nanotube probe tips for atomic force microscopy. *J. Phys. Chem. B* **2001**, *105*, 743−746.

(8) Berber, S.; Kwon, Y.-K.; Tománek, D. Unusually high thermal conductivity of carbon nanotubes. *Phys. Rev. Lett.* **2000**, *84*, 4613.

(9) Saito, R.; Dresselhaus, G.; Dresselhaus, M. S. Trigonal Warping Effect of Carbon Nanotubes. *Phys. Rev. B* **2000**, *61*, 2981−2990.

(10) Saito, R.; Kataura, H. In *Carbon Nanotubes: Synthesis, Structure, Properties and Applications*; Dresselhaus, M. S., Dresselhaus, G., Avouris, P., Eds.; Springer Series in Topics in Applied Physics; Springer-Verlag: Berlin, 2001; Vol. 80, pp 213−246.

(11) Kataura, H.; Kumazawa, Y.; Maniwa, Y.; Umezu, I.; Suzuki, S.; Ohtsuka, Y.; Achiba, Y. Optical Properties of Single-Wall Carbon Nanotubes. *Synth. Metals* **1999**, *103*, 2555−2558.

(12) Dresselhaus, G.; Pimenta, M. A.; Saito, R.; Charlier, J.-C.; Brown, S. D. M.; Corio, P.; Marucci, A.; Dresselhaus, M. S. On the $\pi-\pi$ overlap energy in carbon nanotubes. In *Science and Applications of Nanotubes*; Tománek, D., Enbody, R. J., Eds.; Proceedings of the International Workshop on the Science and Applications of Nanotubes, Michigan State University, East Lansing, MI, July 24−27, 1999; Kluwer Academic: New York, 2000; pp 275−295.

(13) Jishi, R. A.; Venkataraman, L.; Dresselhaus, M. S.; Dresselhaus, G. Phonon Modes in Carbon Nanotubules. *Chem. Phys. Lett.* **1993**, *209*, 77−82.

(14) Kürti, J.; Kresse, G.; Kuzmany, H. Dynamics, dynamical systems, lattice effects, quantum solids, etc. − First-principles calculations of the radial breathing mode. *Phys. Rev. B* **1998**, *58*, R8869.

(15) Sanchez-Portal, D.; Artacho, E.; Soler, J. M.; Rubio, A.; Ordejón, P. Ab initio structural, elastic, and vibrational properties of carbon nanotubes. *Phys. Rev. B* **1999**, *59*, 12678−12688.

(16) Jorio, A.; Souza Filho, A. G.; Dresselhaus, G.; Dresselhaus, M. S.; Saito, R.; Hafner, J. H.; Lieber, C. M.; Matinaga, F. M.; Dantas, M. S. S.; Pimenta, M. A. Joint density of electronic states for one isolated single wall carbon nanotube studied by resonant Raman scattering. *Phys. Rev. B* **2001**, *63*, 245416-1−245416-4.

(17) Odom, T.; Hafner, J. H.; Lieber, C. In *Carbon Nanotubes: Synthesis, Structure, Properties and Applications*; Dresselhaus, M. S., Dresselhaus, G., Avouris, P., Eds.; Springer Series in Topics in Applied Physics; Springer-Verlag: Berlin, 2001; Vol. 80, pp 173−212.

(18) Souza Filho, A. G.; Jorio, A.; Hafner, J. H.; Lieber, C. M.; Saito, R.; Pimenta, M. A.; Dresselhaus, G.; Dresselhaus, M. S. Electronic transition energy E_{ii} for an isolated (*n*, *m*) single-wall carbon nanotube obtained by anti-Stokes/Stokes resonant Raman intensity ratio. *Phys. Rev. B* **2001**, *63*, 241404R.

(19) Yu, Z.; Brus, L. E. Rayleigh and Raman scattering from individual carbon nanotube bundles. *J. Phys. Chem.* B **2001**, *105*, 6831−6837.

(20) Jorio, A.; Souza Filho, A. G.; Dresselhaus, G.; Dresselhaus, M. S.; Swan, A. K.; Ünlü, M. S.; Goldberg, B. B.; Pimenta, M. A.; Hafner, J. H.; Lieber, C. M.; Saito, R. *G*-band resonant Raman study of 62 isolated single wall carbon nanotubes. *Phys. Rev. B* **2002**, *65*, 155412.

(21) Jorio, A.; Souza Filho, A. G.; Brar, V. W.; Swan, A. K.; Ünlü, M. S.; Goldberg, B. B.; Righi, A.; Hafner, J. H.; Lieber, C. M.; Saito, R.; Dresselhaus, G.; Dresselhaus, M. S. Polarized Resonant Raman study of isolated single-wall carbon nanotubes symmetry selection rules, dipolar and multipolar antenna effects. *Phys. Rev. B Rapid* **2002**, *65*, 121402(R).

(22) Tuinstra, F.; Koenig, J. L. Raman Spectrum of Graphite. *J. Chem. Phys.* **1970**, *53*, 1126−1130.

(23) Thomsen, C.; Reich, S. Double resonant Raman scattering in graphite. *Phys. Rev. Lett.* **2000**, *85*, 5214.

(24) Saito, R.; Jorio, A.; Souza Filho, A. G.; Dresselhaus, G.; Dresselhaus, M. S.; Pimenta, M. A. Probing phonon dispersion relations of graphite by double resonance Raman scattering. *Phys. Rev. Lett.* **2002**, *88*, 027401.

(25) Souza Filho, A. G.; Jorio, A.; Samsonidze, Ge. G.; Dresselhaus, G.; Dresselhaus, M. S.; Swan, A. K.; Ünlü, M. S.; Goldberg, B. B.; Saito, R.; Hafner, J. H.; Lieber, C. M.; Pimenta, M. A. Probing the electronic trigonal warping effect in individual single-wall carbon nanotubes using phonon spectra. *Chem. Phys. Lett.* **2002**, *354*, 62−68.

AR0101537